EFAL: EDRS Feeder Link from Antarctic Latitudes

- Preliminary Results of Site Investigations, Availability, and System Requirements

Dirk Giggenbach
Ricardo Barrios
Florian Moll
Ramon Mata Calvo
Sergei Bobrovskyi
Felix Huber

Institute of Communications and Navigation (IKN)
and German Space Operations Center (GSOC),
German Aerospace Center (DLR)
82234 Wessling, Germany
dirk.giggenbach@dlr.de

Nighat F.D. Johnson-Amin

International Polar Foundation (IPF)

Frank Heine
Mark Gregory

Tesat Spacecom

***Abstract*—Laser communications from ground to geostationary satellites can enable high-rate data repatriation from remote ground station sites. When employing Arctic or Antarctic ground hubs, the low link elevations impose a major challenge due to the strong atmospheric index-of-refraction turbulence impact and increased attenuation. The usability of the European Data Relays System (EDRS) for data uplinks from an Antarctic ground station has been analyzed in terms of cloud-availability and feasibility in terms of atmospheric turbulence. For model-verification, an on-site wavefront measurement campaign has been carried out. This scenario also serves as worst test-case for future optical GEO-feeder links**

Keywords—Optical geostationary feeder link; low elevation atmospheric propagation; wavefront quality measurement; focal speckle pattern

I. INTRODUCTION

The European Data Relay System (EDRS) consists of a GEO space segment, able to receive optical BPSK modulated payload data from Earth observation satellites at up to 1.8Gbps. This unique space-asset can also be used for data repatriation from a polar X-band or S-band ground hub, which otherwise would not have a high-rate data link. DLR is investigating the feasibility of such a high-speed data uplink from an optical ground station located in the Antarctic, to double the Earth observation data throughput capacity together with its northern hemisphere counterpart [1]. The major challenge of this low-elevation (10°) optical uplink is the long atmospheric path in the lower link section, imposing strong index-of-refraction turbulence (IRT) effects onto the laser beam. Investigations of beam propagation show that the uplink beam wander necessitates increased beam divergence together with increased transmit power to ensure illuminating the GEO satellite's position. However, the exact quantification of this effect is delicate due to the uncertainty in the turbulence profile over the Antarctic landscape. In this paper we present preliminary results of availability-assessment of an *EDRS Feeder link from Antarctic Latitudes* (EFAL) in terms of cloud-blockage, and theoretical C_n^2-profile estimations as well as in-situ measurements of the Fried-parameter. For the later, a measurement campaign was carried out in the vicinity of the Princess Elizabeth Antarctic Station (PEA) near the Antarctic coast, using the method of tilt-removed short-term focal speckle pattern size statistics [2]. This measurements campaign to our knowledge is the first time that the wavefront statistics have been evaluated for such low elevations on the Antarctic continent.

II. LINK SCENARIO FROM ANTARCTIC OGS

A. EDRS optical link system parameters

The feeder link from Arctic latitudes will connect to Laser Communication Terminals (LCTs) embarked on three different GEO stationary satellites. On the GEOs, the LCT is a part of a hybrid optical- RF payload for data relay. The LCT is serving as input section for RF payloads that have different capabilities regarding the programs:

Alphasat Mission: The data output of the LCT [3] is directly connected to a 600Mbit Ka-band modulator (transparent connection).

EDRS Mission: The data output of the LCT is forwarded to a framing, encrypting and coding group. Due to the resulting overhead, the data volume is increased and dumped through *n* Ka-band channels, each with 600Mbps data rate. The ground segment performs decoding, decryption and de-framing.

Copyright (C) ICSOS2014. All Rights Reserved.

The two scenarios are presented in more detail in Fig. 1. The data from a mass memory of a LEO satellite is RS encoded. In order to prepare the data for the optical ISL (OISL) between a LEO and a GEO satellite, framing and additional RS encoding is performed. A repetition code increases the data rate from 600 Mbps to 1800 Mbps for the LCT. After optical transmission, the GEO LCT receives the data and decodes the repetition code.

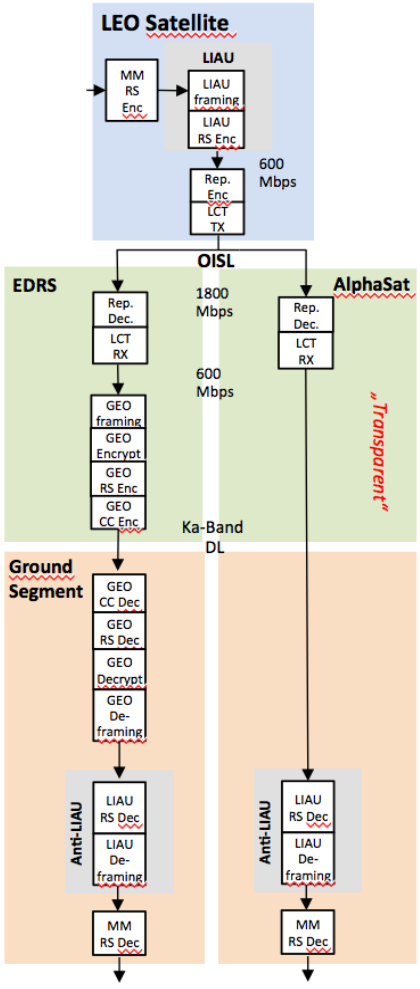

Fig. 1. Hybrid optical-RF payload for data relay for different missions.

In contrast to the transparent Alphasat mission, the data is further processed for the Ka-band downlink at the EDRS spacecraft. Framing and encryption is followed by an RS and convolutional coding stage. After Ka-band downlink the ground segment performs decoding and error correction.

In case of an optical uplink, the optical ground station acts as a LEO satellite. LIAU framing of the user data needs to be applied, even for the transparent Alphasat mission.

In Fig. 2 the GEO LCT and the Ka-band antenna mounted on the Alphasat satellite are shown. In Fig. 3 the EDRS-A LCT is presented being mounted in a TV chamber at Tesat Spacecom during acceptance tests.

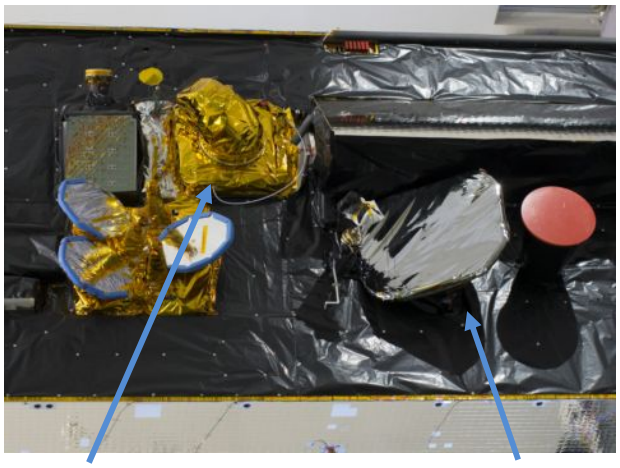

Fig. 2. LCT on earth deck of Alphasat Satellite and dedicated Ka antenna.

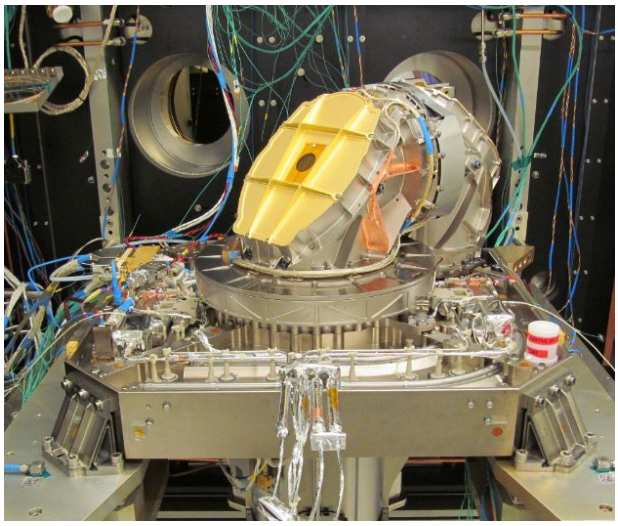

Fig. 3. EDRS-A LCT during acceptance tests in TV chamber at Tesat Spacecom.

B. Geographic situation to EDRS-satellites

Figure 1 shows the orbital positions as well as visibility contours (0° and 10° elevation) of both EDRS spacecraft, EDRS-A being a hosted payload aboard the EUTELSAT 9B satellite. Additionally, the figure shows orbital position of the Alphasat satellite which could also be used for investigations of the optical link quality. All aforementioned spacecraft are visible under 10° elevation from a narrow strip of Antarctic coast stretching approximately between 12°E and 28°E. The range of options for a possible OGS location can be widened if the visibility of only one EDRS spacecraft is considered sufficient.

Copyright (C) ICSOS2014. All Rights Reserved.

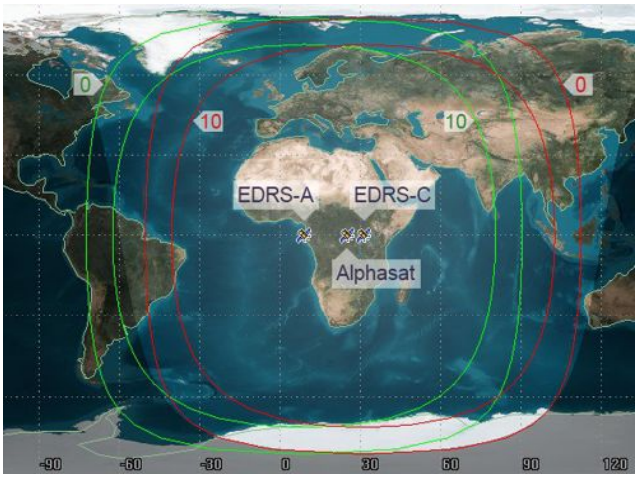

Fig. 4. Orbital positions as well as visibility contours for 0° and 10° elevation of the EDRS spacecraft (green – EDRS-A, red – EDRS-C). The orbital position of the Alphasat satellite is also shown. The Antarctic coastline east and west of +20° longitude sees these GEO-satellites at more than 10° elevation.

C. *Isoplanatic angle versus point ahead*

The geometric situation in an optical link to a geostationary satellite is defined mainly by three angles: the uplink beam divergence, the point-ahead-angle (PAA, typical 18µrad for a geostationary satellite) due to the relative velocity of the satellite versus the optical ground station (OGS), and the isoplanatic angle (IPA) of the atmospheric index-of-refraction turbulence structure. The uplink beam divergence should be made as small as possible to produce the highest signal intensity at the satellite. However, the IRT-induced turbulent beam spread sets a lower limit to this angle. When pointing the laser beam towards the satellite, the atmospheric beam-wander should be compensated be tracking the angle-of-arrival (AoA, caused by IRT) of a reference signal from the satellite, and pointing the outgoing beam accordingly. However, here the IPA sets a limit, as incoming and outgoing beams travers through different atmospheric volumes when IPA<PAA. While the magnitude of the IPA depends on the local IRT-profile structure and the wavelength, this condition is usually the case for low link elevations, as here the IPA becomes very small (figure 5). This leads to the situation, that the observed AoA can no longer serve as reference for pointing the uplink beam in the correct direction to compensate atmospheric beam-wander deviations. Instead, the beam-wander must be balanced by increasing the uplink beam divergence. This effect causes a challenging link-budget in any low-elevation satellite-uplink, requiring very high transmit powers from ground. The quality of pointing-by-tracking has been analyzed and verified in another OGS-GEO measurement campaign [4].

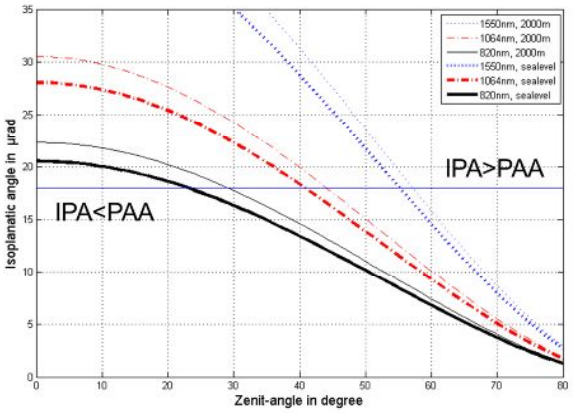

Fig. 5. Isoplanatic angle over zenith-angle for typical IRT-profiles. At 10° elevation (80° zenith angle) in all cases IPA<<PAA (compare with the horizontal line at PAA=18µrad for a geostationary satellite).

D. *Fried-parameter estimation from focal speckle patterns*

To estimate the turbulence conditions at a given OGS-site one can measure the Fried-parameter r_0 as statistical value of the wavefront distortion. Here we utilized the focal speckle pattern method as described in [2] to estimate r_0 by measuring short-term tilt removed values of focal speckle sizes from stars at daytime (Antarctic summer). This method furthermore allows to assess the short-term quality of heterodyning-efficiency to rate the quality of a coherent receiver. In EFAL we employed a 9¼ inch (235mm) aperture telescope with a focal length of 2350 mm to record videos of the focal speckle patterns. Figure 6 shows two examples of focal speckle patterns for good and bad IRT-situation under 10° elevation. Values are collected with an optical band-pass around 600nm wavelength and later converted for the target-wavelength of 1064nm. When using method [2] with stars as reference sources the atmospheric dispersion must be taken into account, leading to a vertically elongated speckle pattern whose size is depending on filter bandwidth and elevation [5][6]. According to [5], for our measurement scenario we have to expect angular dispersion of up to 5µrad.

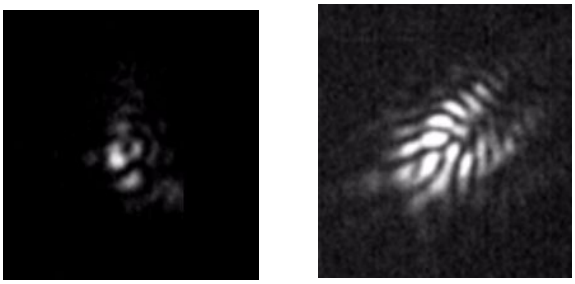

Fig. 6. Example of a small focal speckle pattern due to a large Fried parameter (left), and a bad IRT-situation, causing a large focal speckle pattern (right); measured during EFAL Antarctic r_0 measurement campaign Dec'13-Feb'14.

Copyright (C) ICSOS2014. All Rights Reserved.

III. CLOUD COVER STATISTICS

The presence of clouds in the line of sight can prohibit the optical link due to exorbitantly high attenuation. For water cloud types like Cumulus, Stratus, Stratocumulus, Altostratus, and Nimbostratus this may be as high as 100 up to 600 dB/km and even the thinnest Stratus and Stratocumulus clouds bear over 30 dB of total attenuation [7]. Ice clouds attenuate less. Typical values are 1-6 dB/km and 1-15 dB of total attenuation [8]. Thus, only very thin water clouds and ice clouds bear attenuation low enough to be included in a link margin. However, in most cases the link is totally blocked. Therefore, a statistical analysis of cloud cover occurrence of the particular site must be performed in the planning phase of any ground-satellite laser communication link. Studies do exist, for instance for sites and networks in Europe [7][12], USA [9][10][14], and Japan [11]. Antarctic clouds in the troposphere were examined in general in [17], but not investigated yet addressing link availability. Herein, different kinds of data base for cloud cover estimation are discussed: surface-based observations, airborne measurements and satellite passive/active remote sensing all having particular advantages and disadvantages which are, however, not under discussion here.

Passive remote sensing data is most often used. GEO satellite images from GOES-West, GOES-East, GOES-9, Meteosat-7, and Meteosat-5 were used in [9] to asses link availability for a world spanning ground station network for Deep-Space links. The same image sources together with the measurements from the GEO MTSAT were applied in [10] to estimate worldwide distributed ground stations and network availability for LEO downlinks and Deep-Space links. MTSAT data was also applied to assess availability of LEO-downlinks to the Japanese region [11]. Records from the LEO NOAA satellites were used in [7] to estimate HAP (High-Altitude-Platform)-ground link availability. MSG and METOP images were used in [12] for analysis of satellite down-links in Europe. Active remote measurements from a LEO LIDAR (CALYPSO) and passive measurements from MSG data were used in [13] to derive attenuation with co-aligned LIDAR/camera data for ground stations in Europe. Ground observations, also quite wide spread, were used in [14] to estimate single and joint site availabilities, again for a Deep-space link.

This actual preliminary study shall give a first estimate for expected availability for a particular Antarctic site. The long term mean cloud coverage is the first parameter of interest and therefore investigated here. Neither long term surface-based observations nor airborne measurements at PEA do exist. The Terra (launch 1999, local equatorial crossing time ~10:30 a.m.) and Aqua satellites (launch 2002, local equatorial crossing time ~1:30 p.m.) with MODIS (Moderate Resolution Imaging Spectroradiometer) on board are polar orbiting and have big data availability and are therefore first choice for this preliminary analysis. Also the METOP satellites with the AVHRR/3 (Advanced Very High Resolution Radiometer) would be suitable. As active sensors, also polar orbiting CloudSat with the CPR (cloud profiling radar) and CALIPSO with the CALIOP (Cloud-Aerosoal LIDAR with Orthogonal Polarization) are available. However, these just bear low spatial sampling and therefore, only monthly or seasonal statistics are meaningful [17]. MODIS data is chosen because of a large available data base, easy access of the necessary data products, reasonable spatial resolution (1° grid map resolution) and good visibility from PEA. The MODIS Level 3 Atmosphere Products (MOD08 [15][16]) are selected and herein the parameter for Mean Cloud Fraction. The mean cloud cover at PEA over the year derived from Terra data is shown in Fig. 7. The values are based on 10 year of images, 2000-2009.

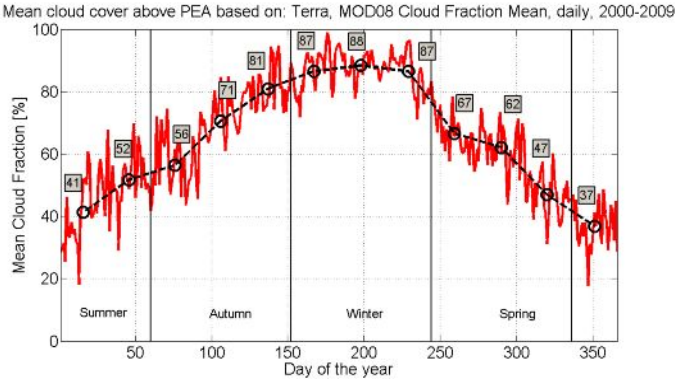

Fig. 7. Course of the year of cloud cover over PEA. Ten years of MODIS data MOD08 are used. The solid red line denotes mean cloud fraction for the day of the year, the black dashed line the according monthly averages.

The seasonal variation is clearly visible. In the winter, cloud cover can be as high as 88 % (monthly average for July), allowing only very limited link times. However in spring, autumn and especially in summer, cloud occurrence decreases significantly allowing monthly averaged link times up to 63 %. The yearly mean cloud cover is depicted in Fig. 8. The overall mean cloud occurrence is 65 %. However, this appears to have considerable high deviation amongst the individual years. Yearly means of up to 71 % occur two times out of ten years and the best year bears 61 % coverage.

The next steps of this PEA cloud cover analysis are the comparison with the Aqua measurements to identify a diurnal tendency if existing. Furthermore, ground observations with higher temporal resolution shall be analyzed as plausibility check and calculation of temporal statistics.

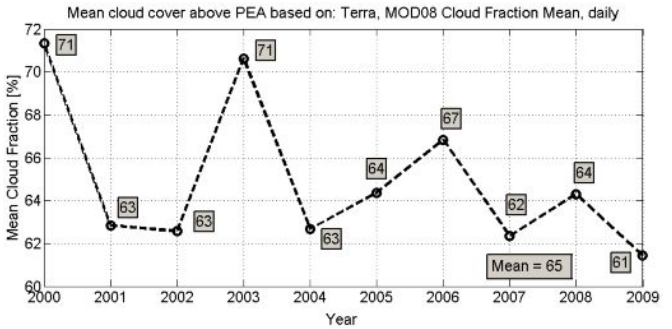

Fig. 8. Course of cloud cover over PEA over the years.

Copyright (C) ICSOS2014. All Rights Reserved.

IV. Turbulence Profile and Analytical Link Fluctuation Assessment

The atmospheric turbulence can be defined by the strength of the fluctuations in the refractive-index, represented with the refractive-index structure parameter C_n^2 in units of $m^{-2/3}$. Along the optical propagation distance the value of C_n^2 has small variations for horizontal paths, while for slant and vertical paths these variations become significant. When a vertical path is considered, the behavior of C_n^2 is conditioned by temperature changes along the different layers within the Earth's atmosphere; hence, the refractive-index structure parameter becomes a function of the altitude above ground.

Many authors have tried to predict the behavior of the refractive-index structure parameter, and various models have been proposed. However, it should be noted that most of these models are based on fittings from experiments conducted in specific places, which makes difficult their generalization. The most widespread model is the Hufnagel-Valley, best suited for inland daytime and nighttime conditions. Unfortunately, currently there is no standard model of C_n^2 profile for Antarctic locations.

A. *Theretical C_n^2-profiles PEA-OGS and other Antarctic locations*

Concerning Antarctic locations most of the literature dealing with the atmospheric quality focus on the *seeing* parameter, which is a scaled version of the Fried parameter given in units of arcseconds, usually measured at zenith for a 550nm wavelength [18][19][20]. Regarding C_n^2 profile measurements at Antarctic locations the literature is rather limited and only a few references are available [19][21]. Masciadri et al. [21] using validated simulations by means of mesoscale models have produced a series of nighttime C_n^2 profiles for three different locations in the Antarctic continent, namely Dome A, Dome C and South Pole. Fig. 9 reproduces the data from [21] including the altitude for each of the locations plotted.

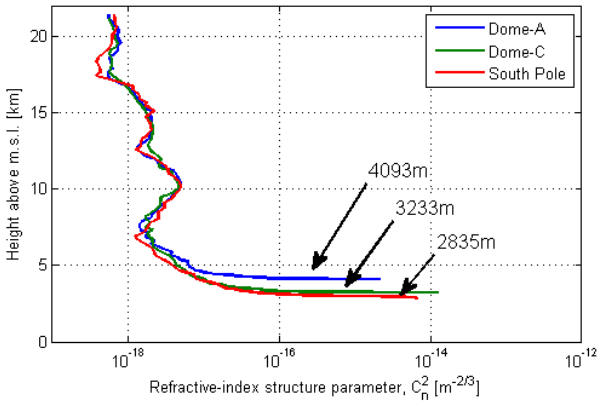

Fig. 9. Median C_n^2 vertical profiles simulated with a mesoscale model for Dome A, Dome C and South Pole, including the altitude a.m.s.l. of each location.

If there is an initial estimation for the C_n^2 profiles at Antarctic latitudes, a particular expression could be fitted to this data in order to obtain a suitable model to make an extrapolation for what could be the situation at Princess Elizabeth Antarctica station. For the sake of versatility we chose the C_n^2 Izaña model [22], due to their multiple defining parameters. The expression for the nighttime Izaña model used in this work is given by

$$C_n^2(h) = \begin{cases} C_{n0}^2 \left(\frac{h}{h_s}\right)^{-2/3} ; & h \le h_s \\ C_{n0}^2 ; & h_s < h < h_i \\ C_{n0}^2 \exp\left(\frac{h_i}{h_r}\right)\exp\left(-\frac{h}{h_r}\right) + C_{nl}^2 \exp\left(-\frac{h}{h_l}\right) + \\ 12 C_{nl}^2 W^2 \left(\frac{h}{h_t}\right)^{10} \exp\left(-\frac{10h}{h_t}\right); & h > h_i \end{cases}, \quad (1)$$

where h is the height above the terrain; h_s is the surface layer height; C_{n0}^2 is assumed uniform throughout the inversion layer extending between the heights h_s and h_i; h_r is the space constant for the transition between the inversion layer and the free atmosphere; C_{nl}^2 is the structure parameter for free atmosphere; h_l is the height characterizing the exponential fall-off in the free-atmosphere region; W is the root-mean-squared wind velocity averaged over the 5 to 20 km altitude interval, and h_t is the tropopause height. It shall be noted that in original reference, the constant scaling factor for the last term in Eq. (1) is 3 instead of the value 12 used in this paper, which was found to produce a better fit to the C_n^2 profiles presented by Masciadri et al. [21]. The daytime version of Eq. (1) can be found in [22], along with a more detailed explanation of the defining parameters.

Using the Izaña nighttime model a fit was made to the profiles for Dome A, Dome C and South Pole. Then, using the fitted model an extrapolation of the C_n^2 profile is made to the conditions of the PEA station and the resulting profile at plotted in Fig. 10, where the model fitted to the South Pole C_n^2 profile given by [21] is also shown as reference.

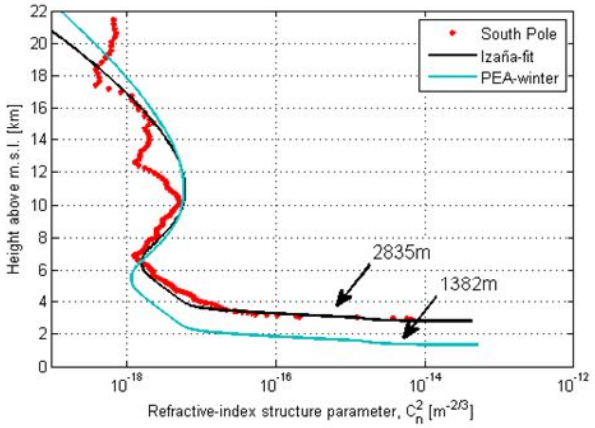

Fig. 10. South Pole C_n^2 profile (red dots), the fitted Izaña model (solid black line) to the South Pole profile, and the extrapolation made from the Izaña model to the expected conditions at PEA (solid blue line) for nighttime - i.e. Antarctic winter - inlcuding the altitude a.m.s.l. of each location.

Copyright (C) ICSOS2014. All Rights Reserved.

Additional to the extrapolation of the Izaña model for PEA station at nighttime conditions, i.e. Antarctic winter, the same strategy was followed to provide a daytime, i.e. Antarctic summer, version of the PEA C_n^2 profile under the assumption that during the summer the refractive-index structure parameter C_n^2 value at ground level and the surface layer height h_s should be larger than in winter time. TABLE I. gives the assumed parameter values used for the definition of the C_n^2 profile at PEA station for nighttime and daytime conditions, all other parameters of the Izaña model not shown in the table are set the default values given in [22].

TABLE I. PARAMETER VALUES IN THE IZAÑA MODEL FOR THE ASSUMPTIONS MADE FOR GENERATING C_N^2 PROFILE AT PEA STATION UNDER NIGHTTIME AND DAYTIME CONDITIONS.

Condition	Corresponding Izaña model parameters			
	C_{n0}^2 [$m^{-2/3}$]	h_s [m]	C_{nl}^2 [$m^{-2/3}$]	h_t [m]
Winter	$1.5 \cdot 10^{-15}$	200	$1.2 \cdot 10^{-17}$	9600
Summer1	$9.0 \cdot 10^{-11}$	200	$1.0 \cdot 10^{-16}$	9600
Summer2	$2.0 \cdot 10^{-11}$	400	$1.0 \cdot 10^{-16}$	9600

B. *Expected IRT-Related Parameter Ranges*

Once a set of C_n^2 profiles have been selected, a more detailed analysis can be done regarding the IRT effects on a OGS-GEO optical uplink, for which the elevation angle is 9º under the EFAL scenario.

The Fried parameter measures the integrated turbulence strength along the optical path through the atmosphere, where smaller r_0 values correspond to larger atmospheric index-of-refraction turbulence. The Fried parameter is given by [23]

$$r_0 = \left[0.42 \sec(\zeta) k^2 \int_{h_0}^{H} C_n^2(h) dh \right]^{-3/5}, \qquad (2)$$

where ζ is the zenith angle, $k=2\pi/\lambda$ is the wavenumber and λ is the wavelength; h_0 is the OGS altitude and H is the GEO satellite height.

On the other hand, beam wander $\langle r_c^2 \rangle$ measures the average displacement of the beam at the receiver from the boresight, while the angular beam wander gives the same information but referred as an angular tilt at transmitter side. The beam wander can be calculated as [23]

$$\left\langle r_c^2 \right\rangle = 0.54 (H - h_0)^2 \sec(\zeta) \left(\frac{\lambda}{2W_0} \right)^2 \left(\frac{2W_0}{r_0} \right)^{5/3}, \qquad (3)$$

where W_0 is the beam radius at the transmitter plane.

Both the Fried parameter and angular beam wander expected behavior are presented in Fig. 11, where other locations than PEA are show for reference.

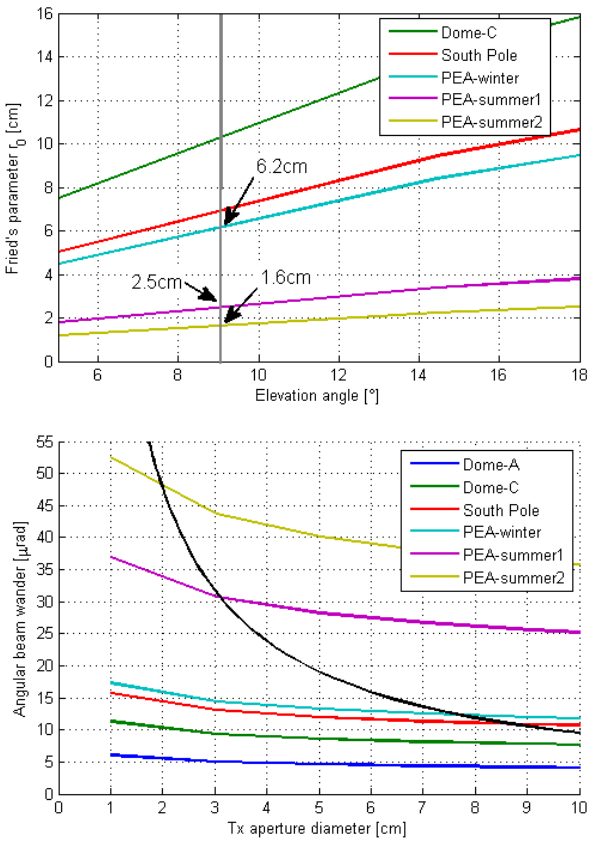

Fig. 11. Fried parameter r_0 vs. elevation angle (top plot) for different Antarctic C_n^2 profiles. The 9º elevation angle for the EFAL scenario is indicated by a gray vertical line, and the corresponding r_0 value is shown for the turbulence profiles for PEA station. Angular beam wander (botton plot) vs. transmitter aperture diameter for different Antarctic C_n^2 profiles. The black line represents the points where the angular beam wander has the same value as the difraction limited half-angle beam divergence.

The expected on-axis scintillation index (SI) in the uplink for a tracked beam at 9º elevation angle is presented in Fig. 12, where it is noteworthy that the SI for the two summer profile models at the PEA station are practically the same. This is due the fact that the scintillation process is mostly influenced by turbulence above the surface layer height, and for these two models the upper part the C_n^2 profile was chosen to be characterized by the same value as shown in TABLE I. It should be noted that the on-axis SI value is rather constant for the smallest transmitter aperture diameters up to 10cm, regardless of the turbulence profile used in the calculations with the corresponding change in SI value. The expression for the SI used to produce Fig. 12 can be found in Chapter 12 of [23].

Copyright (C) ICSOS2014. All Rights Reserved.

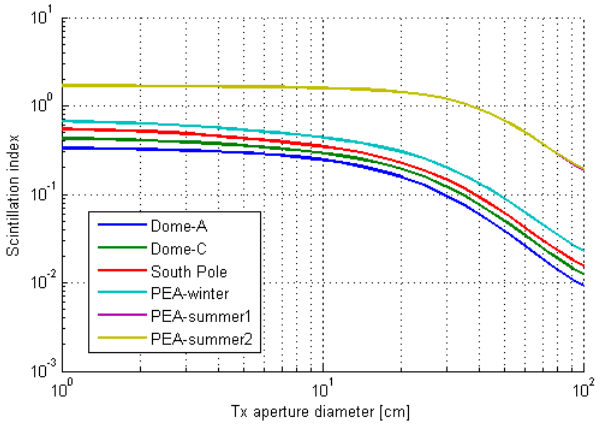

Fig. 12. On-axis uplink scintillation index for tracked beam for different Antarctic C_n^2 profiles, at 9º elevation angle corresponding to the EFAL scenario. Note that the curves for PEA-summer1 and PEA-summer2 are overlapping.

V. Fried-Parameter Measurement Campaign at Antarctic Station

To confirm theoretical parameter ranges and substantiate the understanding of low-elevation wavefront distortion, a measurement campaign at the Princess Elizabeth Station was prepared and carried out in the Antarctic Summer 2013/14.

A. Focal Camera Measurement Setup

The instrument assembled to measure the Fried parameter r_0 at Princess Elizabeth Antarctic station consist primarily of a Celestron CPC Goto telescope with an aperture diameter of 235mm and 2350mm focal length, which produces a focal ratio (F-number) of 10. The imaging device is a Skyris 445M Monochrome CCD camera with square pixels of size 3.75µm. Along with the camera a red color filter centered at 633nm and 100nm bandwidth was used, in order to reduce the background noise due to the blue sky. Additionally, the instrument makes optional use of a Barlow lens that can effectively increase the focal length of the telescope by a factor of 2.25.

The limit of maximum resolution offered by the complete system is determined through the diffraction limited Airy disk zero-ring diameter D_{Airy}, which is given by

$$D_{Airy} = 2.44 \cdot \lambda \cdot f / D_{aperture} , \qquad (4)$$

where f is the effective focal length (2.35m without, and 5.29m with the Barlow). Thus, the minimum possible Airy pattern in the focal point of the telescope, at the central wavelength of the red color filter, becomes 34.8µm and 15.5µm when the Barlow lens is installed or not, respectively. These values translate for the CCD camera images into a diffraction limited Airy pattern of 9 and 4 pixels in diameter, which should be enough for obtaining reasonable estimations of the Fried parameter r_0.

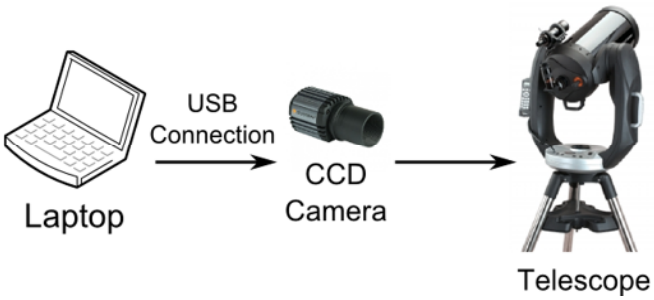

Fig. 13. Schematic diagram for the intrument setup used during the EFAL r_0 measurement campaign Dec'13-Feb'14 at Princess Elizabeth Antarctica Station.

B. Measurement Campaign at the Antarctic Station

To record the focal speckle pattern videos the brightest stars visible from the station's location were used, namely Betelgeuse and Procyon for elevations around 10°, and Sirius, Antares, and Rigel for higher elevations.

The measurement campaign at PEA encountered several difficulties associated with setting up and using a telescope not designed for field use in an exposed setting, at very low temperatures. Additionally the adverse weather in the Antarctic summer 2013/14 with long periods of storm and cloud cover limited the gathering of a higher number of measurements. More challenges were imposed by the strong wind causing vibrations to the telescope tube that prevented proper focusing. Moreover, the calibration of the telescope attitude was difficult as it required finding reference stars at daytime, as the sun was not setting during the whole measurement period. However, the resulting measurements proved very valuable in the end, and regarding the limited budget and short preparation time for the campaign, the outcome is conclusive.

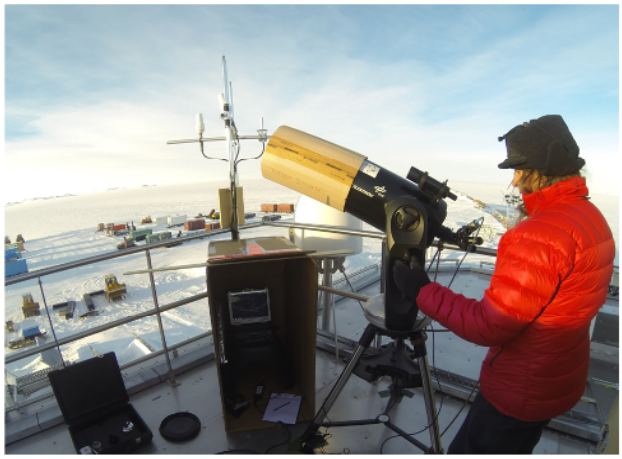

Fig. 14. Typical situation during focal speckle pattern measurements at PEA. The provisional cardboard tube was required during calibration with the Sun as reference object.

C. Preliminary results summary of r_0-measurements

The meteorological conditions for the Antarctic summer season 2013/14 were exceptionally bad, considerably reducing the available measuring time due to cloud blockage and strong

Copyright (C) ICSOS2014. All Rights Reserved.

haze concentration on the horizon, which limited low elevation measurements options. Nevertheless, it was possible to obtained low elevation (about 10º) r_0 measurements for two different days, and four days for higher elevation.

Available data is presented as a boxplot in 15, where the lower and the upper edges of the box represents the 25th and 75th percentile, respectively; the center red line is the median, and the whiskers extend to the most extreme data points not considered outliers, and outliers are plotted individually as red crosses.

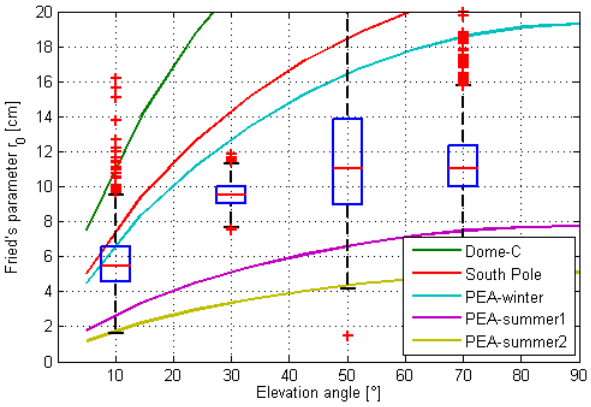

Fig. 15. Box plot from in-situ Fried parameter for different elevation angles, during EFAL Antarctic r_0 measurement campaign Dec'13-Feb'14. Theoretical estimations for PEA station and other Antarctic location are also shown for reference.

It readily seen in Fig. 15 that the uncertainty in the *in-situ* Fried parameter r_0 estimation is rather high, due to the low number of measurements available. Albeit this inconvenient situation, some trends can be identified in the data.

For the analysis of Fig. 15 it has to be taken into that all data for 10º elevation angles was taken when the sun was between 9 and 10º above the horizon. This scenario will place the r_0 estimated values closer to the nighttime conditions, as it can be seen most left boxplot where the median r_0 is closer to the estimation for PEA in winter. The same happens for the 30º elevation data, which was taken with a sun elevation of 7º above the horizon. For the rest of the measurement points the elevation of the sun above the horizon was between 10 and 24º, which should produce somewhat smaller r_0 values than the predictions for nighttime but still higher values than those for daytime, that we estimated assuming the worst possible conditions.

Following the previous reasoning, a possible explanation for the data points in Fig. 15 - to be laid between the daytime and nighttime preliminary assumption for PEA station - is that the sun elevation was not either at its maximum or below the horizon, which cannot be regarded as limiting conditions as the ones assumed when estimating the PEA C_n^2 profile for winter and summer condition, i.e. nighttime and daytime, respectively.

VI. Results and Uplink Assessment

Using the preliminary results from the EFAL r_0 measurement campaign during the Antarctic summer 2013/14, the evaluation of the Fried parameter at 10º elevation resulted in a minimum and maximum value of 1.6 and 9.5cm, respectively; while the median value was 5.5cm. As it is clearly seen in Fig. 15, the minimum r_0 value falls close to the PEA-summer1 turbulence profile estimation; the median value approaches the PEA-winter estimation, and the maximum r_0 value improves the best assumption for PEA station falling close to the Dome C predictions for the Antarctic winter.

It is noteworthy that results are heavily depending on the geographic location and time of the day, as the meteorological situation changes with ground altitude and prevailing wind directions and strength strongly depends on geographic topology.

The expression for the average optical power P_R detected at distance L is given by

$$P_R = P_T G_T \tau_T \tau_A S G_R \tau_R L_T \,, \tag{5}$$

where P_T is the transmitted average power from a source with aperture diameter D_T and full-angle divergence $\theta_T=2\lambda\sqrt{8}/\pi D_T$, $G_T=16/\theta_T^2$ and $G_T=(\pi D_R/\lambda)^2$ are the transmitter and receiver gains, respectively; τ_T and τ_R are transmitter and receiver efficiencies, respectively; $S=(\lambda/4\pi L)^2$ is the free-space loss, and $L_T=\exp(-G_T\theta_{mp}^2)$ corresponds to the miss-pointing loss, where θ_{mp} is the angular beam wander.

Using (5) one can optimize the transmitter aperture diameter in order to obtained the lowest possible losses in the optical link, provided that all other parameters are set fixed. In the EFAL scenario where transmission is to be done with EDRS GEO satellite, which will be equipped with a next generation laser communication terminal (LCT), the receiver aperture set to D_R=13.5cm, the link distance is L=40655km, and the receiver sensitivity for bit error-rate of 10^{-8} at 600Mbps data rate, using BPSK modulation, is established to be -51dBm [3].

Adjusting the transmitter aperture diameter D_T and knowing the expected value of the Fried parameter r_0, for the specific EFAL scenario, results in a coupled loss between the beam divergence - which defines the spreading loss - and beam wander loss. Such relation can readily be seen in (5). Fig. 16 shows the estimated optical transmitter aperture size under different turbulence conditions defined by the *in-situ* r_0 measurements at PEA station.

Copyright (C) ICSOS2014. All Rights Reserved.

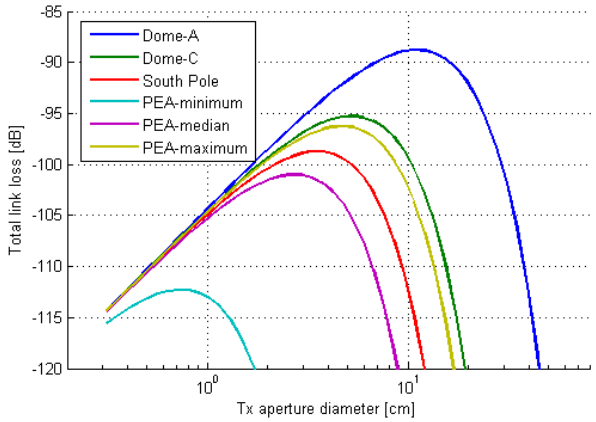

Fig. 16. Total link loss vs. transmitter aperture diamter estimated from *in-situ* measurements of the Fried parameter at Princess Elizabeth Antarctica station, for an optical uplink to a GEO satellite at 9º elevation. Other Antarctic locations are shown as reference.

Once an optimum size of the transmitter aperture diameter D_T has been found, a link budget calculation for EFAL scenario can be made. All the pertinent parameters and calculations are presented in TABLE II. where all the parameter values included in the final link budget calculations are shown in bold face.

TABLE II. LINK BUDGET CALCULATIONS FOR MINIMUM, MEDIAN AND MAXIMUM FRIED PARAMETER VALUES ESTIMATED FROM IN-SITU MEASUREMENTS AT PRINCESS ELIZABET ANTARCTICA STATION. ALL VALUES IN THE TABLE ARE GIVEN IN DECIBELS UNLESS OTHERWISE NOTED.

Parameter	**Fried parameter r_0 value @ 1064nm**		
	minimum 1.5cm	***median 5.5cm***	***maximum 9.5cm***
Tx aperture diameter [cm]	0.72	2.70	4.72
Tx antena gain	**83.54**	**95.02**	**99.87**
Tx optical loss	**-3.00**	**-3.00**	**-3.00**
Free-space loss	**-293.63**	**-293.63**	**-293.63**
Atmospheric loss	**-3.00**	**-3.00**	**-3.00**
Spreading loss	**-1.34**	**-1.39**	**-1.41**
Beam wander loss	**-3.82**	**-3.85**	**-4.05**
Rx antenna gain	**112.01**	**112.01**	**112.01**
Rx optical loss	**-3.00**	**-3.00**	**-3.00**
Total link loss	**-112.26**	**-100.85**	**-93.23**
Rx Sensitivity BER=10^{-8}	**-51.00**	**-51.00**	**-51.00**
Required Tx power [dBm]	**61.26**	**49.85**	**45.23**
Required Tx power [W]	1338.09	96.70	33.34

It becomes evident by inspecting the required transmitter power, in the EFAL framework, that the atmospheric turbulence imposes a major obstacle to achieve an operational system, as for coherent communication it is not possible to use transmitter spatial diversity to obtain the required transmitter power for a worst case scenario - i.e. when the Fried parameter is r_0=1.6cm. Although, it seems to be possible to meet power requirements for the best case scenario (r_0=9.5cm) with current amplifier technology for 1064nm. For the case of the median value of r_0=5.5cm it should be possible to obtained additional gain by means of state-of-the-art forward error correction (FEC) code schemes

ACKNOWLEDGMENT

DLR acknowledges the financial support of the Bavarian Ministry of Economic Affairs and Media, Energy and Technology for the Antarctic measurement campaign.

REFERENCES

[1] S. Bobrovskyi, R. Barrios, D. Giggenbach, F. Moll, F. Sellmaier, F. Huber, “EFAL: EDRS Feeder Link from Antarctic Latitudes – System Architecture and Operations Concept,” submitted to SpaceOps 2014, 13th International Conference on Space Operations.

[2] D. Giggenbach, “Deriving an estimate for the Fried parameter in mobile optical transmission scenarios,” Applied Optics, Vol. 50, No. 2,. Optical Society of America, Jan. 2011, p. 222-226

[3] G. Muehlnikel, H. Kämpfner, F. Heine, H. Zech, D. Troendle, R. Meyer and S. Philipp-May, “The Alphasat GEO Laser Communication Terminal Flight Acceptance Tests,” in Proc. International Conference on Space Optical Systems and Applications (ICSOS), 2012.

[4] Ramon Mata Calvo, Peter Becker, Dirk Giggenbach, Florian Moll, Malte Schwarzer, Martin Hinz, Zoran Sodnik, ”Transmitter Diversity Verification on Artemis Geostationary Satellite,” Proceedings of the SPIE, Vol. 8971, Free-Space Laser Communication and Atmospheric Propagation XXVI, February 2014

[5] D. Peach “Atmospheric dispersion and its effect on high resolution imaging”, Journal of the British Astronomical Association 122, 4, 2012

[6] R.J. Scaddan, J.C. Dainty, “A simple method of estimating the RMS phase variation due to atmospheric turbulence”, Optics Communications, Vol. 21, 1, April 1977

[7] F. Moll and M. Knapek, “Wavelength selection criteria and link availability due to cloud coverage statistics and attenuation affecting satellite, aerial, and downlink scenarios,“ in Proceedings of SPIE, vol. 6709, 2007, pp. 670916-1 - 670916-12.

[8] J. H. Churnside, K. Shaik, “Atmospheric Propagation issues relevant to optical communications,” NOAA Technical Memorandum ERL WPL-159, Boulder, Colorado, 1989.

[9] G. S. Wojcik, H. L. Szymczak, R. J. Alliss, R. P. Link, M. E. Craddock, and M. L. Mason, “Deep-Space to ground laser communications in a cloudy world,“ in Proceedings of SPIE, vol. 5892, 2005, pp. 589203-1 - 589203-11.

[10] R. J. Allis and B. Felton, “The mitigation of atmospheric impacts on free-space optical communications,“ in Proceedings of ICSOS 2012, Ajaccio, Corsica, France, 2012.

[11] Y. Takayama, M. Toyoshima, and N. Kura, “Estimation of accessible probability in a low Earth orbit satellite to ground laser communications,” in Radioengineering, Volume 19, Issue 2, pp. 249-253, 2010.

[12] F. Lacoste, A. Guerin, A. Laurens, G. Azema, C. Periard, and D. Grimal, “FSO ground network optimization and analysis considering the influence of clouds,“ in Proceedings of the 5th European Conference on Antennas and Propagation, 2011, pp. 2746 - 2750.

[13] S. Poulenard, M. Ruellan, B. Roy, J. Riédi, F. Parol, and A. Rissons, “High altitude clouds impacts on the design of optical feeder link and optical ground station network for future broadband satellite services,” presentation given at LASE, SPIE Photonics West, Conference 8971: Free-Space Laser Communication and Atmospheric Propagation XXVI, San Francisco, California, USA, to be published in Proceedings of SPIE, vol. 8971, 2014.

[14] H. Hemmati: Deep Space Optical Communications. Hoboken: Wiley & Sons, 2006.

Copyright (C) ICSOS2014. All Rights Reserved.

[15] M. D. King, J. Closs, S. Wharton, and M. Myers, “EOS Data Products Handbook Volume 1 Revised 2004,” NASA Goddard Space Flight Center, Greenbelt, Maryland, USA, 2004.

[16] C. L. Parkinson and R. Greenstone, “EOS Data Products Handbook Volume 2,” NASA Goddard Space Flight Center, Greenbelt, Maryland, USA, 2000.

[17] D. H. Broomwich et al., "Tropospheric clouds in Antarctica," in Review of Geophysics, vol. 50, 2012.

[18] W. Saunders, J. S. Lawrence, J. W. Storey and M. C. Ashley, “Where is the best site on Earth? Domes A, B, C and F, and Ridges A and B,” Publ. Astronom. Soc. Pac., Vol. 121, pp. 976-992, 2009.

[19] H. Trinquet, A. Agabi, J. Vernin, M. Azouit, E. Aristidi and E. Fossat, “Nighttime Optical Turbulence Vertical Structure above Dome C in Antarctica,” Publ. Astronom. Soc. Pac., Vol. 120, pp.203-2011, 2008.

[20] J. S. Lawrence, M. C. Ashley, A. Tokovinin, and T. Travouillon, “Exceptional astronomical seeing conditions above Dome C in Antarctica,” Nature, Vol. 431, pp. 278-281, 2004.

[21] E. Masciadri, F. Lascaux and S. Hagelin, “Optical turbulence: site selection above the internal antarctic plateau with a mesoscale model,” in Proceedings of SPIE, vol. 7733, pp. 77334F, 2010.

[22] A. Comerón, F. Dios, A. Rodríguez, J. Rubio, M. Reyes and A. Alonso, “Modeling of Power Fluctuations Induced by Refractive Turbulence in a Multiple-Beam Ground-to-Satellite Optical Uplink,” in Proceedings of SPIE, vol. 5892, pp.58920O, 2005

[23] L. Andrews and R. Phillips, *Laser Beam Prpagation through Random Media*, 2nd ed., Bellingham: SPIE Press, 2005.

Copyright (C) ICSOS2014. All Rights Reserved.